Characterizing Laser Preheat for Laser-Driven Magnetized Liner Inertial Fusion Using Soft X-Ray Emission

D. H. Barnak,[1] M. J. Bonino,[1] P.-Y. Chang,[2] J. R. Davies,[1] E. C. Hansen,[3] D. R. Harding,[1] J. L. Peebles,[1] and R. Betti[1]

[1]Laboratory for Laser Energetics, University of Rochester
[2]Institute of Space and Plasma Sciences, National Cheng Kung University
[3]Department of Physics and Astronomy, University of Rochester

Introduction

MagLIF (magnetized liner inertial fusion) is a magnetized target fusion scheme utilizing a cylindrical implosion with an axial magnetic field to compress preheated deuterium–tritium fuel to fusion-relevant densities and temperatures. The magnetic field mitigates the radial conduction losses and allows these implosions to happen ~3× slower than direct or indirect laser fusion spherical implosions. The lower volume decrease with equal convergence ratios for cylinders versus spheres requires that the fuel start at a much higher temperature than in traditional inertial confinement fusion schemes. This is accomplished by using an axial laser to heat the fuel via inverse bremsstrahlung absorption prior to the implosion. In both the laser-driven and pulsed-power versions of MagLIF, the gas in the cylinder is held in by a thin window at the top that the laser must burn through to heat the gas. The most important aspects about preheat to quantify are the gas temperature as a function of time, mix due to the window being pushed into the implosion region by the preheat beam, mix due to wall ablation into the gas, and how the initial axial magnetic field affects the preheat. Characterizing the preheat process is critical to the success of MagLIF as described in several publications.[1–4]

For the laser-driven MagLIF design, a 1.84-μm polyimide foil window was used to cover the laser entrance hole (LEH) and contain the ~10 atm of $2\%_{at}$ Ne-doped D_2 gas inside a parylene-AF4 ($C_8H_4F_4$) cylinder. To study the LEH window disassembly in terms of laser transmission, backscatter, sidescatter, and x-ray emission, a series of LEH foil-only shots was performed along the axis of a single beam of the OMEGA laser. LEH window shots were performed in two configurations: one to measure backscatter, sidescatter, and transmission using Beamline 25 and the other to measure transmission and forward scatter using Beamline 46. The Beamline 25 configuration was then used to heat the gas cylinders. Dante, an array of K-edge–filtered x-ray diodes, was used to measure the total x-ray flux from the LEH window disassembly, which is proportional to the laser energy absorbed by the window. The temperature of the gas in the front 1 mm of the cylinder was also measured by Dante after the window had expanded and cooled. The temperature of the wall and the gas in the implosion region was measured using a three-channel K-edge–filtered soft x-ray imager (SXR). Each configuration is illustrated in Fig. 1. Six cylinders in total were shot: two with an initial 15-T magnetic field and an initial gas density of 1.5 mg/cm^3; two without a magnetic field at the same gas density; one at 1/2 the initial gas density; and one at 3/2 the initial gas density. The transmission, backscatter, and sidescatter data from the LEH window and cylinder shots are summarized in another publication,[5] whereas the x-ray emission and radiation temperature are presented in this summary alongside plasma temperature measurements of the gas and the wall of the cylinder as a function of time.

Analysis of LEH Window Disassembly Using Dante

An array of filtered x-ray diodes called Dante[6] was used to characterize the x-ray spectrum and total energy of x rays emitted by the exploding window during the laser pulse. Each diode in the array has its own aperture, filter, signal cable, electrical attenuator, power tee, and transient digitizer. The combination of all of these components is referred to as a channel. Traditionally, 11 channels are employed to diagnose radiation temperatures for hohlraums. This makes Dante ideal to use for diagnosing both the LEH window-only shots and the full-cylinder preheat shots. Voltage signals from Dante are used to recover both time-resolved and time-integrated spectra of an emitting plasma.

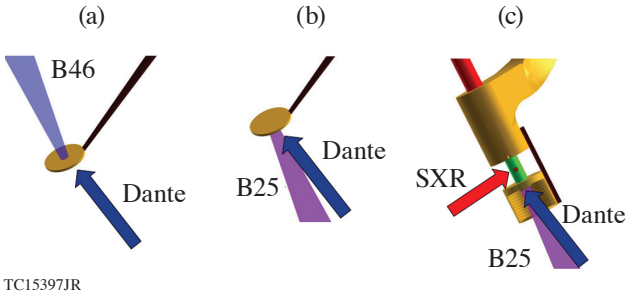

Figure 1
Two opposing lasers of the OMEGA Laser System, (a) Beamline 46 and (b) Beamline 25, were used to illuminate a standalone LEH window to measure the window forward transmission, backscatter, and soft x-ray emission to track the window disassembly. (c) A Ne-doped D_2 gas inside a fluorinated plastic cylinder with an identical LEH window and a diagnostic side window drilled out of it was then heated using Beamline 25 to measure the preheat temperature over time.

With limited signal information and a unique amalgam of elements present in the plasma, several well-established methods of recovering the x-ray spectrum are impossible to employ.[7,8] A cubic-spline spectral unfold technique[9] was used to recover information about the total radiated power and infer the total x-ray power-emitted from the LEH window. Time-integrated x-ray spectra from the LEH window-only shots show only a marginal increase in total x-ray energy emitted by the exploding window with increasing laser energy. This is consistent with the laser absorption and backscatter measurements that do not change significantly with laser energy.[5] The total x-ray energy is found by integrating the recovered time-integrated spectrum over photon energy. The error bars on the results shown in Fig. 2 were calculated analytically according to the cubic-spline interpolation algorithm.[9]

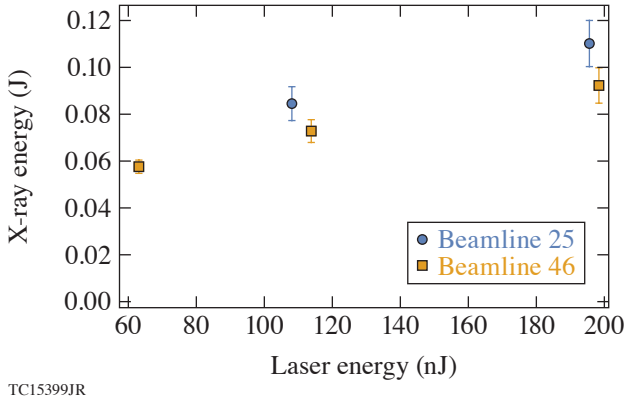

Figure 2
A summary of the x-ray energy emitted in nanojoules as a function of the laser energy incident on the LEH window-only targets. Total x-ray energy emitted by the foil is minimal and changes very little with respect to initial laser energy incident on the foil. The x-ray energy incident on Dante is also affected by which beam configuration is used. Dante looks directly at the laser–foil interaction in the Beamline 25 configuration, whereas it is blocked by the foil in the Beamline 46 configuration.

1. Comparison of Dante Data from LEH Window Shots to 2-D Simulations

Dante can also be used to verify hydrocode results for the LEH foil-only experiments. The four channels provide an entire spectral range pertinent to both the continuum and line emission relevant to polyimide plastic, and a high confidence in the plasma conditions predicted by hydrocodes can be established by direct comparison.

The output of two codes, *FLASH* and *DRACO*, is post-processed using *Spect3D* detailed atomic modeling to produce a spectrum.[10] The spectrum is then convolved with the instrument and filter response functions to produce synthetic x-ray diode traces that can be compared to the data, seen in Figs. 3 and 4. For the window-only shots, *FLASH* is able to predict the plasma conditions well enough to reproduce the x-ray diode data across all channels with a margin no larger than 30%. *DRACO* can reproduce time-integrated spectra very well, but it cannot reproduce individual channel curves to the same accuracy as *FLASH*.

The discrepancy between these two codes and the experiment alludes to a mechanism of channel formation that expands and pushes away the plasma generated by the laser–window interaction, thereby limiting the amount of laser energy absorbed by the window. Despite better agreement, *FLASH* overpredicts the laser absorption in the window at ~30%, with similar LEH burn-through times, window material propagation speed, and preheat temperatures predicted by *DRACO*. The analysis of the window x-ray emission is in good agreement with previously published data[5] that indirectly measured laser absorption, which is shown in Fig. 5. This suggests that the source of the overestimation in both codes is missing physics.

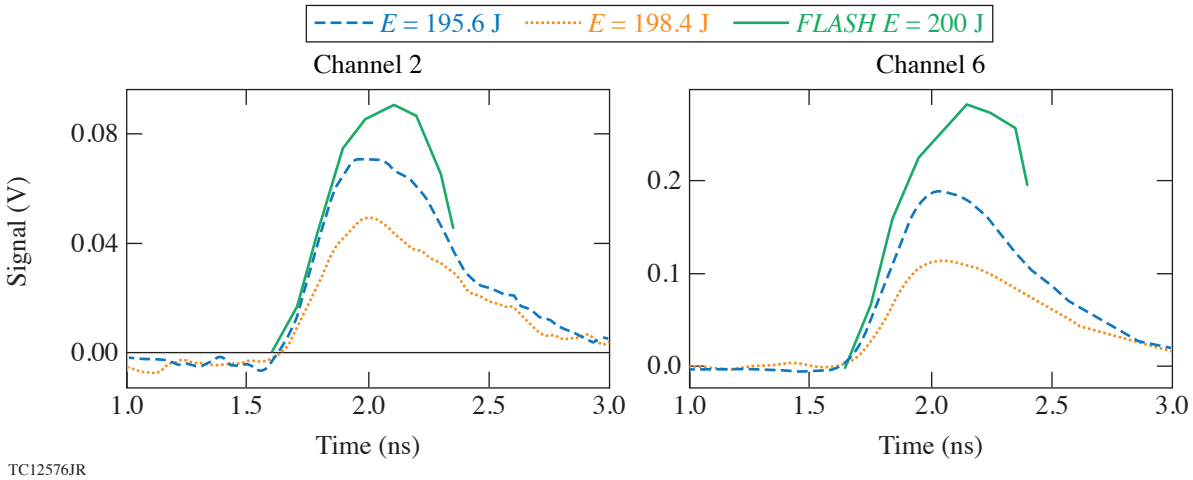

Figure 3
X-ray diode data compared to results from post-processing the 2-D hydrocode *FLASH* using *Spect3D* detailed atomic physics. The agreement between data and simulation across all x-ray diode channels is within a margin no larger than 30%.

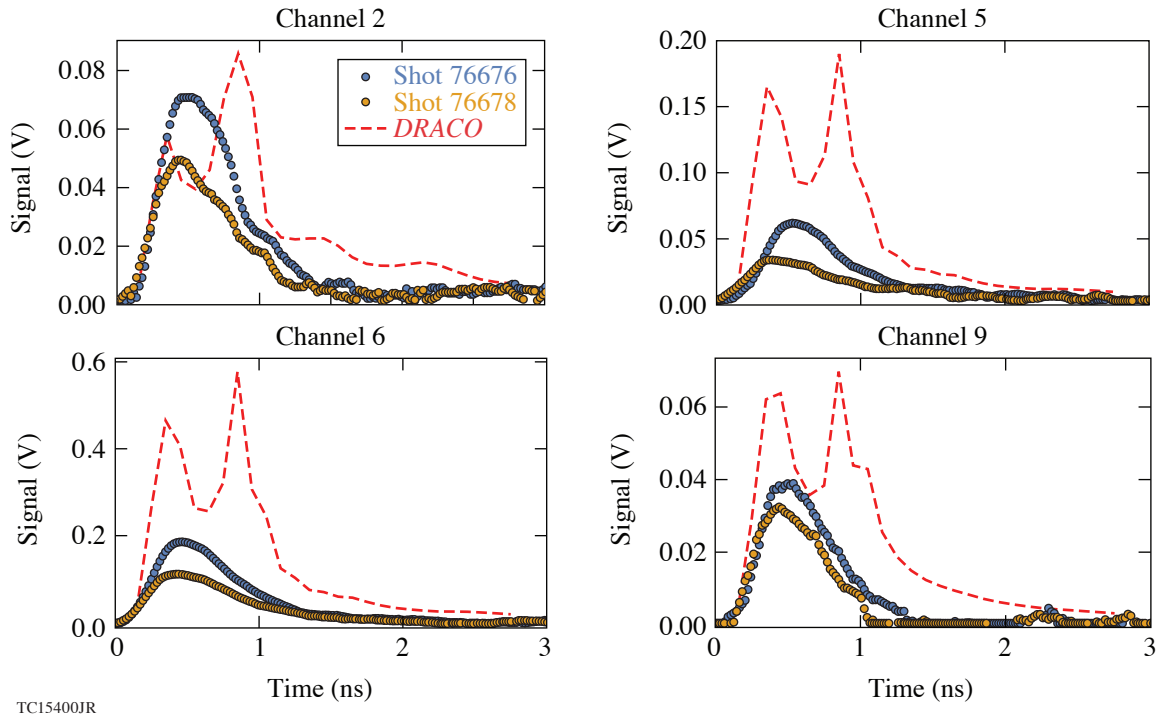

Figure 4
DRACO simulation results compared to Dante experimental data. The laser energy used in the simulation is 200 J, 195.6 J for shot 76676, and 198.4 J for shot 76678.

2. Inferring Gas Temperature from Dante Measurements of Cylinders

The viewing angle of Dante to the cylinder targets suggests that the first 1 mm of the target, which includes a region of gas outside of the implosion region, can be seen by Dante. A schematic view of the Dante line of sight is shown in Fig. 6. The neon doping in the gas should contribute to the x-ray spectrum in a region easily measurable by Dante, so that a gas temperature can be recovered from Dante from specific channels. Simulations from *DRACO* are used to decompose each channel into fractional contributions to the signal in each channel from the window, wall, and gas.

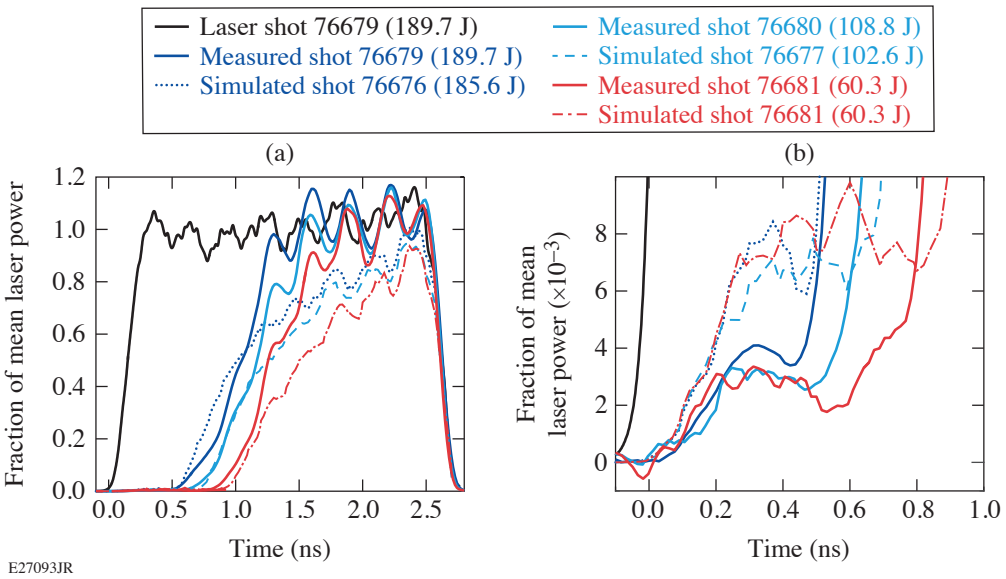

Figure 5
The laser transmission as a function of time is shown for (a) the entirety of the laser pulse and (b) at the start of the pulse in better detail. The laser absorption in the window early in time is overestimated in the simulation, but the simulations and experiments show that laser absorption is independent of the incident laser power. The experiments show the transmitted laser light quickly growing to the full power of the laser pulse, whereas the simulations reach full power only toward the end of the pulse.[5]

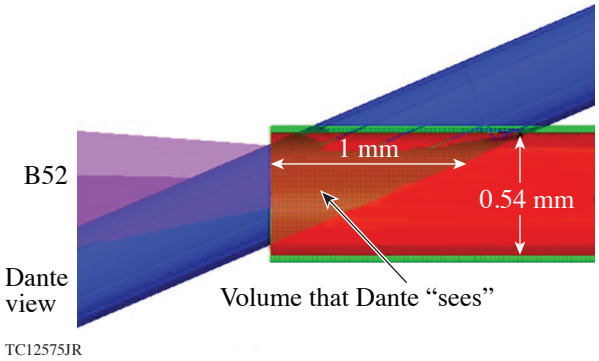

Figure 6
Schematic view of the Dante view down the cylinder. Dante is able to see emission from the gas as far as 1 mm into the cylinder.

To avoid issues concerning opacity, a series of three simulations from *DRACO* was post-processed in *Spect3D* considering x-ray emission from the wall only; the wall and the window; and the wall, window, and gas. A self-consistent decomposition of the percent contribution from wall, window, and gas of the signal in each channel is made. Select channels are shown decomposed into the three possible contributors along with the raw data of the corresponding channel in Fig. 7.

Based on the signal decomposition of Channel 9 from Fig. 7, times between 1.1 and 2.2 ns were considered to be the best times to compare spectra for gas emission. Instead of comparing signals convolved with instrument response functions, the adaptive cubic spline unfold method can be used to compare spectra recovered from Dante directly with *Spect3*D simulation results from *DRACO*. The spectral power emitted must be a function of electron temperature in the gas, and the data from the *DRACO* simulation are used to construct a conversion function of the form

$$k_{T_e} + b_{T_e} P_9 = T_e, \tag{1}$$

which takes the spectral power in the Channel 9 region, P_9, and calculates the electron temperature T_e. Both k_{T_e} and b_{T_e} are free-fitting parameters with associated errors σ_k and σ_b. The spectral power over the Channel 9 region for the cubic-spline unfold is

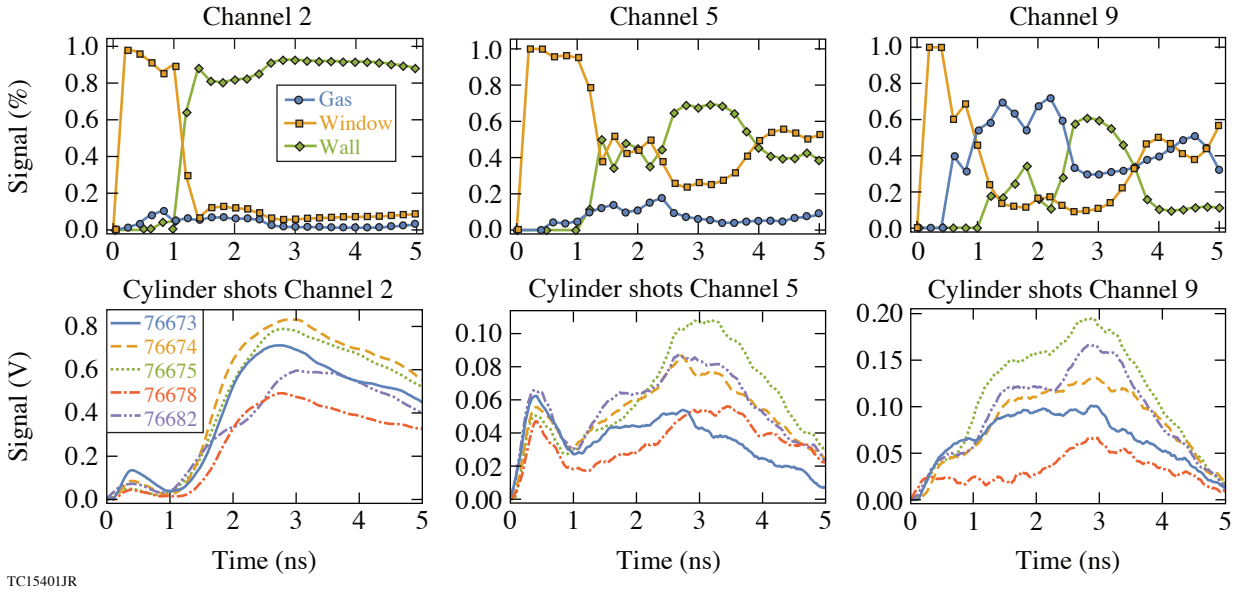

Figure 7
Decomposed signals from Channels 2, 5, and 9 are shown in percent contributions from the window, wall, and gas using results from *DRACO* post-processed in *Spect3D*. This is compared to the raw signals from the respective channels to determine the composition of the signal at different times. Lower-photon-energy channels show only window and wall emission, whereas higher-energy channels have most of their signal contributed by the gas in the front 1 mm of the cylinder. This allows Dante to be used to estimate a time-resolved gas temperature measurement.

then plugged into Eq. (1) to recover a measurement of electron temperature. The resulting error of the total calculation takes into account the error propagation of the cubic spline and the standard error of the linear model fit

$$\sigma_{T_e}^2 = \left(b_{T_e} P_9\right)^2 \left[\left(\frac{\sigma_b}{b_{T_e}}\right)^2 + \left(\frac{\sigma_{P_9}}{P_9}\right)^2\right] + \sigma_k^2, \tag{2}$$

where σ_{P_9} is the associated error in spectral power calculated analytically from the cubic spline.[9] The comparisons between experimentally inferred gas electron temperature and predictions by *DRACO* between 1.0 and 2.1 ns are shown in Fig. 8. The temperature from *DRACO* is calculated as a volumetric average over the front 0.5 mm of the cylinder for the full cylinder radius. The electron temperature quickly saturates at ~200 eV due to a drop in inverse bremsstrahlung absorption and cooling due to expansion. The ion temperature slowly thermalizes with the electron population. By the end of the laser pulse, the entirety of the cylinder including the implosion region reaches an ion temperature of 200 eV. This confirms the ability of a single OMEGA beam to reach adequate preheating conditions for a MagLIF implosion.

3. Proof of Thermal Conduction Wall Heating Suppression with Magnetic Fields

Another useful result of the signal decomposition technique is the demonstration of the reduction in wall emission and wall heating due to magnetic-field suppression of thermal conduction from the window and the gas. One of the six cylinder shots that was initially magnetized with an ~15-T magnetic field prior to the start of the laser pulse has enough signal in Dante to make a comparison to the two other unmagnetized shots at equal initial gas pressure.

Looking at the signal composition for each channel from Fig. 7, the magnetic field provides an ~20% to 40% reduction in signal for the regions in each channel that correspond to wall emission. Since the portion of the spectrum that contributes to these channels is heavily line dominated, a 20% reduction in signal infers a significant decrease in the temperature of the wall blow-off plasma. The main mechanism in the formation of the wall blowoff is thermal conduction from the hot window plasma and gas into the wall according to 2-D simulations. This implies that the magnetic field limits the amount of thermal energy transfer from

the window and gas to the wall. Looking at Dante signal traces for Channels 2, 5, and 6, where wall emission comprises >50% of the signal in Fig. 9, the case of 15-T initial field sees a reduction in signal by about a factor of 2.

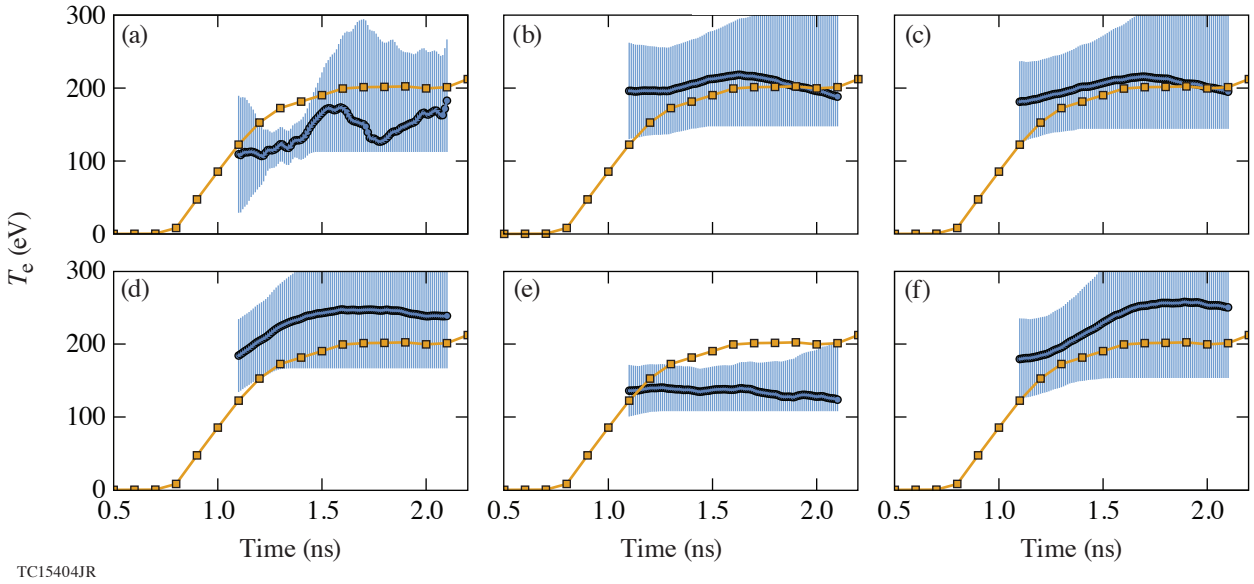

Figure 8
Preheat curves for all six cylinder shots where the squares represent results from *DRACO*. In general, the electron temperature follows the predicted *DRACO* electron temperatures fairly closely, within shot-to-shot variations. Comparisons between [(a), (b)] shots with and [(c), (d)] shots without an initial axial magnetic field show no appreciable difference between electron temperatures. A shot with (e) 5-atm initial pressure shows less preheating than the 10-atm *DRACO* prediction and (f) a shot with a higher initial pressure shows greater preheating than the 10-atm prediction. It can even be implied that (d) has roughly the same initial pressure as (f), although no direct measurement of the gas pressure exists for these two cases.

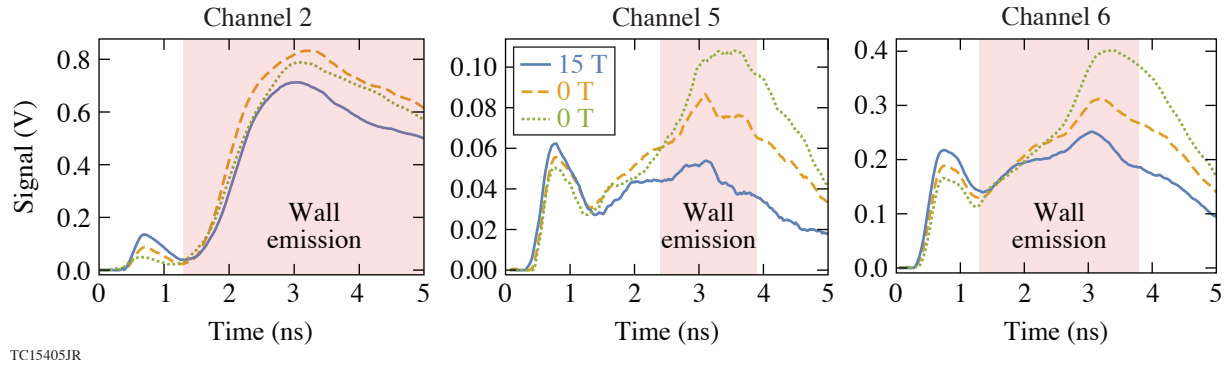

Figure 9
Raw Dante signals for Channels 2, 5, and 6 for the cases of 15 T and 0 T. In every channel where wall emission comprises >50% of the signal (shaded region), the case with 15-T initial field has an ~20% to 40% decrease in signal.

Measuring Gas Temperature in the Implosion Region Using Ne Soft X Rays

The cylinder experiments used a diagnostic window drilled into the side and resealed with a 1.84-μm polyimide film to look at soft x-ray emission from the gas and the wall. Spatially and temporally resolved images of the side diagnostic window are measured using SXR, which is a three-channel differentially filtered imager. The spectral responses of each filtered channel are shown in Fig. 10.

There is no possible way to recover the spectrum of the plasma from these three channels. Furthermore, SXR is not an absolutely calibrated diagnostic, so each channel signal must be compared with another for any useful information to be extracted. Using results from 2-D hydrocodes as a guide, a set of possible 2-D plasma profiles was constructed. The spectrum for each possible combination of temperature and density is calculated using *Spect3D* detailed atomic modeling and then convolved with response functions of SXR to generate a grid of possible solutions. The channel ratios from the data are then converted to temperature and density by using the solution grid under the condition that $T_{gas} > T_{wall}$. Since the system is highly degenerate, the main result from this analysis establishes a lower bound on the possible gas temperature of 100 eV at 1.3 ns into the laser pulse, which is shown in Fig. 11. This result is consistent with the Dante-inferred temperatures toward the front of the cylinder and confirms that the goal of at least a 100-eV preheat is achieved with a single OMEGA laser beam.

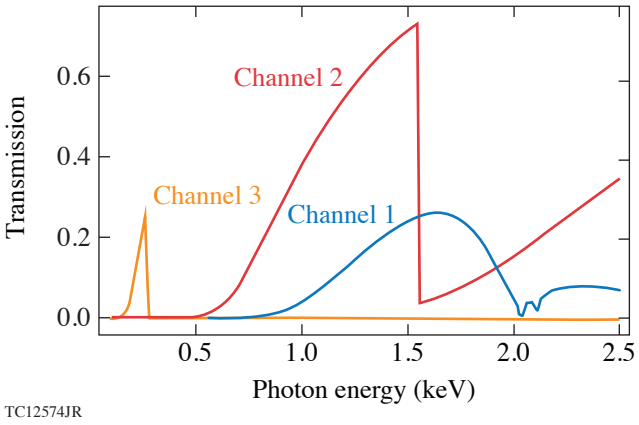

Figure 10
Response functions for the three channels of SXR used to measure preheat temperature.

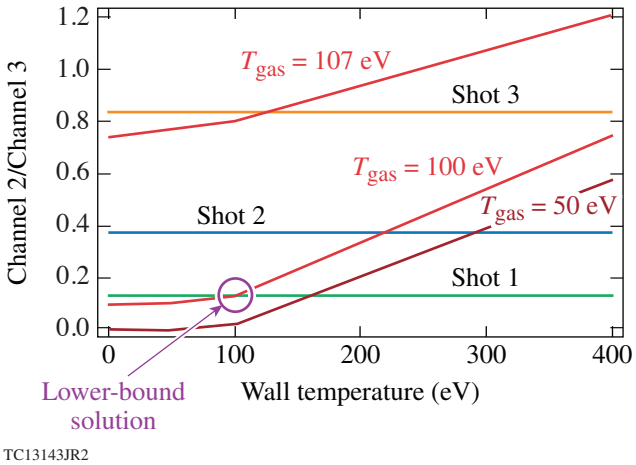

Figure 11
The lower-bound solution for the temperature of the preheated D_2 gas. Other channel ratios give a solution higher than 100 eV. The solutions always find the case where $T_{gas} = T_{wall}$ given the constraint of $T_{gas} \geq T_{wall}$ as shown in the plot.

Conclusions

Measurements of the LEH window disassembly in terms of total emitted x-ray energy demonstrate that there is a small variation of laser light absorbed by the window as a function of the intensity of the laser. This is consistent with results obtained from analysis of the backscatter and sidescatter measurements. Furthermore, both *DRACO* and *FLASH* overpredict the amount of laser energy absorbed by the window during disassembly, and the difference between the two codes suggests that the reason for this may be related to instabilities such as laser self-focusing and ponderomotive pressure applied by the laser field that causes the window to form a channel into the gas. Despite overpredicting the window absorption, the plasma temperature evolution is the same between the simulation predictions and experiment as expected for inverse bremsstrahlung heating. Lower initial gas density is shown to lower the preheat, and higher initial density is shown to raise the total preheat relative to the simulation predictions

for the nominal case. There is no discernible difference between magnetized and unmagnetized preheat in terms of the electron temperature within the shot-to-shot variation and calculated error bars. The plasma temperature in the implosion region has been shown to meet the 100-eV requirement set in the point design specifications, although measuring the time evolution of the laser heating in the implosion region proved to be impossible. Implosion-region measurements are consistent with the measurements made of the front 1 mm of the cylinder and simulation results. The comparisons between the experimental results and simulations indicate that using *DRACO* as a prediction for the design of future preheating schemes is adequate.

The information, data, or work presented herein was funded in part by the Advanced Research Projects Agency-Energy (ARPA-E), U.S. Department of Energy, under Award No. DE-AR0000568, the Department of Energy National Nuclear Security Administration under Award No. DE-NA0003856, and in part under contract 89233218CNA000001, the U.S. Department of Energy Office of Fusion Energy Sciences under award No. DE-SC0016258, the U.S. Department of Energy Office of Inertial Confinement Fusion under Cooperative Agreement No. DE-FC52-08NA28302, the University of Rochester, and the New York State Research and Development Authority. Los Alamos National Laboratory, an affirmative action/equal opportunity employer, is operated by Triad National Security, LLC for the National Nuclear Security Administration of U.S. Department of Energy under contract 89233218CNA000001.

1. A. J. Harvey-Thompson *et al*., Phys. Plasmas **22**, 122708 (2015).
2. M. Geissel *et al*., Phys. Plasmas **25**, 022706 (2018).
3. A. J. Harvey-Thompson *et al*., Phys. Plasmas **26**, 032707 (2019).
4. A. J. Harvey-Thompson *et al*., Phys. Plasmas **25**, 112705 (2018).
5. J. R. Davies *et al*., Phys. Plasmas **25**, 062704 (2018).
6. C. Sorce *et al*., Rev. Sci. Instrum. **77**, 10E518 (2006).
7. R. E. Marrs *et al*., Rev. Sci. Instrum. **86**, 103511 (2015).
8. A. Seifter and G. A. Kyrala, Rev. Sci. Instrum. **79**, 10F323 (2008).
9. D. H. Barnak *et al*., Rev. Sci. Instrum. **91**, 073102 (2020).
10. J. J. MacFarlane *et al*., in *Inertial Fusion and Sciences Applications 2003*, edited by B. A. Hammel *et al.* (American Nuclear Society, La Grange Park, IL, 2003), pp. 457–460.